JACS
JOURNAL OF THE AMERICAN CHEMICAL SOCIETY
Article
pubs.acs.org/JACS

How and When Does an Unusual and Efficient Photoredox Reaction of 2-(1-Hydroxyethyl) 9,10-Anthraquinone Occur? A Combined Time-Resolved Spectroscopic and DFT Study

Jiani Ma, Tao Su, Ming-De Li, Wei Du, Jinqing Huang, Xiangguo Guan, and David Lee Phillips*

Department of Chemistry, The University of Hong Kong, Pokfulam Road, Hong Kong S.A.R., P. R. China

Supporting Information

ABSTRACT: The photophysics and photochemical reactions of 2-(1-hydroxyethyl) 9,10-anthroquinone (2-HEAQ) were studied using femtosecond transient absorption (fs-TA), nanosecond transient absorption (ns-TA), and nanosecond time-resolved resonance Raman (ns-TR^3) spectroscopy techniques and density functional theory (DFT) calculations. In acetonitrile, 2-HEAQ underwent efficient intersystem crossing to the triplet excited state ((2-HEAQ)^3). A typical photoreduction reaction for aromatic ketones took place via production of a ketyl radical intermediate for 2-HEAQ in isopropanol. In water-containing solutions with pH values between 2 and 10, an unusual photoredox reaction reported by Wan and co-workers was detected and characterized. Observation of the protonated species in neutral and acidic aqueous solutions by fs-TA spectra indicated the carbonyl oxygen of (2-HEAQ)^3 was protonated initially and acted as a precursor of the photoredox reaction. The preference of the photoredox reaction to occur under moderate acidic conditions compared to neutral condition observed using ns-TR^3 spectroscopy was consistent with results from DFT calculations, which suggested protonation of the carbonyl group was the rate-determining step. Under stronger acidic conditions (pH 0), although the protonated (2-HEAQ)^3 was formed, the predominant reaction was the photohydration reaction instead of the photoredox reaction. In stronger basic solutions (pH 12), (2-HEAQ)^3 decayed with no obvious photochemical reactions detected by time-resolved spectroscopic experiments. Reaction mechanisms and key reactive intermediates for the unusual photoredox reaction were elucidated from time-resolved spectroscopy and DFT results. A brief discussion is given of when photoredox reactions may likely take place in the photochemistry of aromatic carbonyl-containing compounds and possible implications for using BP and AQ scaffolds for phototrigger compounds.

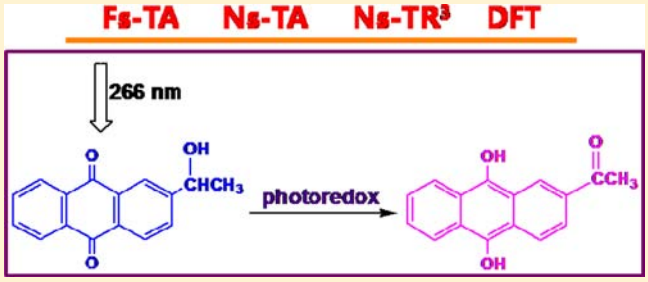

INTRODUCTION

Photoredox reactions for *m*- and *p*-nitrobenzyl alcohols have been previously investigated.[1] However, applications of these photoredox reactions were not extensively studied due to the perceived enigmatic character of the nitro group in organic chemistry.[2] More recently, a novel photoredox reaction was discovered for the more readily available systems benzophenones (BPs) and anthraquinones (AQs).[3]

BPs and AQs are among the most well-known chemically important molecules that can undergo efficient intersystem crossing (ISC) to the triplet excited state.[4−11] Photoreduction reactions of BPs and AQs have been widely studied and reported by many researchers. In recent years, Wirz and co-workers studied the photohydration reaction of BP and found that protonation of the carbonyl oxygen of the BP group contributes to the quenching of the triplet excited BP by protons and may provide a new route to some unusual photoreactions.[12] The photoredox reaction of BPs and AQs discovered by Wan and co-workers can be considered as one example elucidated in the work reported later in this paper.[3] The initial discovery of the photoredox reaction for some BP and AQ molecules revealed that the ketone is reduced to an alcohol and the side chain alcohol moiety is apparently simultaneously oxidized to its ketone form.[3] A time-resolved study on the BP derivative,[13] 3-(hydroxymethyl)benzophenone (*m*-BPOH), demonstrated that *m*-BPOH undergoes the ISC process in aprotic solvent acetonitrile and the conventional photoreduction reaction in strong hydrogen-donor solvents like isopropanol. However, in acidic aqueous solutions, the photohydration reaction is the predominant reaction at pH 0 while the photoredox reaction was found to be the predominant one at pH 2. As a close relative to BP, AQ compounds were also observed to exhibit unusual and highly efficient photoredox reactions.[3e,f] Here, we focus on 2-(1-hydroxyethyl) 9,10-anthraquinone (2-HEAQ) as an illustrative example to investigate the photochemical reactions and especially the photoredox reaction of an AQ system. At first glance the photochemical reaction of this AQ derivative was postulated as a photooxidation. However, via closer inspection one noticed that the reaction generating (2-acetyl) 9,10-anthraquinone as the final product proceeded through an air-

Received: May 8, 2012
Published: August 21, 2012

   dx.doi.org/10.1021/ja304441n | J. Am. Chem. Soc. 2012, 134, 14858−14868

sensitive intermediate under an air-saturated environment (see Scheme 1).[3] In addition, no concentration dependence on the

Scheme 1. Overall Photoredox Reaction of 2-HEAQ Followed by Oxidation with the Final Product 3-Formylanthraquinone

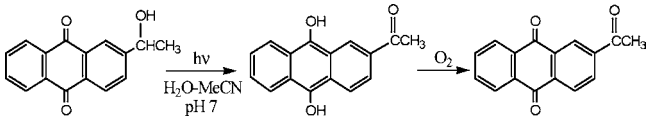

quantum yield was observed over the concentration range from 10^{-6} to 10^{-4} M, suggesting that the reaction was unimolecular with regard to the substrate.[3a] Nevertheless, the reaction mechanism remained uncertain due to the limited information known at the time. First, the photoredox reaction was reported to proceed via an initial deprotonation of the methylene C−H bond followed by protonation of the AQ carbonyl oxygen by water.[3a] In contrast, a later study preferred protonation of the carbonyl oxygen as the first step.[3e,f] The two proposed reaction mechanisms regarding the sequence of the deprotonation and protonation reactions for the photoredox reaction of 2-HEAQ are depicted here in Schemes 2 and 3, respectively.

Scheme 2. Proposed Photoredox Reaction Mechanism of 2-HEAQ That Undergoes Deprotonation First and Followed by a Protonation Reaction[3a]

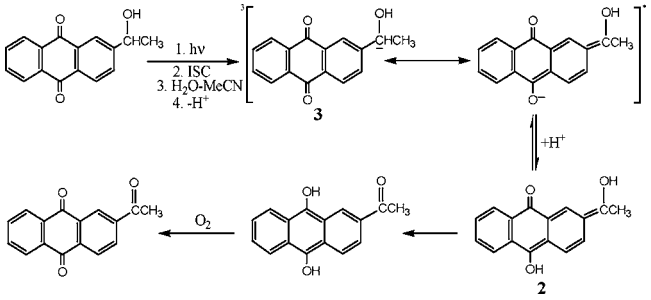

Scheme 3. Proposed Photoredox Reaction Mechanism of 2-HEAQ That Undergoes Protonation First and Then a Subsequent Deprotonation Process[3e,f]

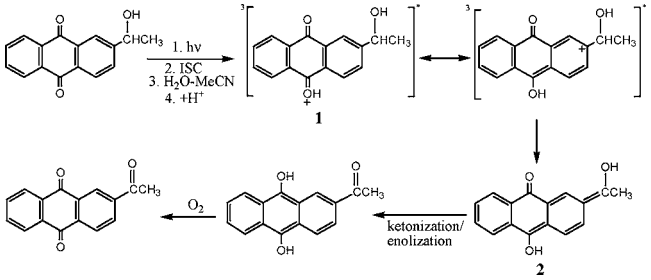

The photochemistry of AQ derivatives in aqueous solutions had also received increasing interest as a new platform for developing photoremovable protecting groups in recent years.[14−16] However, from the earliest example of using an AQ derivative to photorelease a protected galactose by Iwasmura and co-workers[14a] to a recent study employing 2-HEAQ as a photolabile protecting group for carboxylic acids,[15] the mechanism(s) of these deprotection reaction(s) and key reactive intermediates have not yet been elucidated in detail.

We are pleased to report a combined femtosecond transient absorption (fs-TA), nanosecond transient absorption (ns-TA), and nanosecond time-resolved resonance Raman (ns-TR^3) spectroscopic investigation of the photophysics and photochemistry of 2-HEAQ in aqueous solutions with varying pH in an effort to unravel the mechanism(s) and key reactive intermediates of the photoredox reaction and other competing reactions. This work also provides a foundation for future study of photodeprotection reactions utilizing the AQ scaffold. Density functional theory (DFT) calculations were conducted to deepen the interpretation of experimental results. fs-TA experiments for *m*-BPOH were also performed to facilitate a comparison between the photoredox and other reactions that take place in AQ versus BP systems.

EXPERIMENTAL AND COMPUTATIONAL METHODS

2-(1-Hydroxyethyl) 9,10-anthraquinone (2-HEAQ) was synthesized following reported literature methods.[3e] Spectroscopic-grade acetonitrile (MeCN), isopropyl alcohol (IPA), and deionized water were used. Perchloric acid ($HClO_4$) and sodium hydroxide (NaOH) were used to control the sample pH. All of the mixed solvent ratios are volumetric ratios.

A. Femtosecond Transient Absorption (fs-TA) Experiment. fs-TA measurements were performed using a femtosecond regenerative amplified Ti:sapphire laser system. The amplifier was seeded with the 120 fs output from the oscillator. The probe pulse was generated using about 5% of the amplified 800 nm output to generate a white-light continuum (350−800 nm) in a CaF_2 crystal. The probe beam was split into two before passing through the sample. One beam travels through the sample; the other was sent to the reference spectrometer monitoring the fluctuations in the probe beam intensity. Fiber optics were coupled to a multichannel spectrometer. For the present experiments, the 40 mL solution in a flowing 2 mm path-length cuvette was excited by a 267 nm pump beam. Sample solutions for the fs-TA experiments were prepared to obtain an absorbance of 1 at 267 nm; in that way, the same number of photons was absorbed for the same irradiating conditions in each case.[17]

B. Nanosecond Transient Absorption (ns-TA) and Nanosecond Transient Emission (ns-EM) Experiment. ns-TA and ns-EM measurements were carried out on a commercial laser flash photolysis setup. The 266 nm pump laser pulse was obtained from the fourth-harmonic output of an Nd:YAG laser, and the probe light was provided by a 450 W xenon lamp. Sample was excited by the pump laser, and at a right angle the probe light from the xenon lamp was passed through the sample. The two beams were focused onto a 1 cm quartz cell. The transmitted probe light was then measured either by a single detector (for kinetic analysis) or by an array detector (for spectral analysis). The changes in the transmission properties were normally converted into changes of optical density (ΔOD). Signals analyzed by a monochromator were detected by a photomultiplier, and the signal was processed via an interfaced PC and analytical software. Unless indicated, ns-TA experiments were done in air-saturated solutions and sample solutions were prepared with an absorbance of 1 at 266 nm.

C. Nanosecond Time-Resolved Resonance Raman (ns-TR^3) Experiments. ns-TR^3 experiments were performed using the apparatus and methods described previously,[18] and a short description is given. A 266 nm pump wavelength (by the fourth harmonic of a Nd:YAG nanosecond pulsed laser) and the 368.9 nm probe wavelength (by the second anti-Stokes hydrogen Raman-shifted laser line produced from the second harmonic of a second Nd:YAG laser) were used. The pump pulse excited the sample to initiate the photochemical reactions, and the probe pulse interrogated the sample and the intermediate species produced. Laser beams were lightly focused and aligned so that they were overlapped onto a flowing liquid stream of sample. A pulse delay generator was employed to electronically control the time delay between the pump and the

dx.doi.org/10.1021/ja304441n | J. Am. Chem. Soc. 2012, 134, 14858−14868

probe laser. Raman-scattered light was acquired using a backscattering geometry and detected by a liquid nitrogen-cooled charge-coupled device (CCD) detector. The TR^3 signal was acquired for 10 s by the CCD before being read out to an interfaced PC computer, and 10 scans of the signal were accumulated to produce a resonance Raman spectrum. ns-TR^3 spectra were obtained from subtraction of an appropriately scaled probe-before-pump spectrum from the corresponding pump−probe resonance Raman spectrum to remove nontransient bands. Raman bands of MeCN were employed to calibrate the Raman shifts with an estimated accuracy of 5 cm^{-1}. Sample concentrations in ns-TR^3 were $\sim 5 \times 10^{-4}$ M.

D. Density Functional Theory (DFT) Calculations. DFT calculations were done employing the Becke three-parameter hybrid method with the Lee−Yang−Parr correlation functional approximation (B3LYP)[19,20] method with a 6-311G** basis set. Raman spectra were obtained using a determination of the Raman intensities from transition polarizabilities calculated by numerical differentiation, with an assumed zero excitation frequency. A Lorentzian function with a 15 cm^{-1} bandwidth for the vibrational frequencies and a frequency scaling factor[21] of 0.974 was used in the comparison of the calculated results with the experimental spectra. No imaginary frequency modes were observed at the stationary states of the optimized structures, and only one imaginary frequency was observed for the saddle point transition state structures. The photoredox reaction was explored by optimizing the structures of the reactant, transition states, and product complexes. Transition states were located using the Berny algorithm.[22] Frequency calculations at the same level of theory were performed to confirm that the structures were at local minima with all-real frequencies or at transition states with only one imaginary frequency. The nature of the transition states was determined by analyzing the motion by the eigenvector associated with the imaginary frequency. Intrinsic reaction coordinates (IRC)[23] were calculated for the transition states to confirm the relevant structures connect the two relevant minima. TD-DFT methodology is used to compute the low-lying excited states of transient species interested.[24] GaussSum software is utilized to simulate the UV−vis spectra.[25] The polarizable continuum model (PCM) is used for evaluating the (bulk) solvent effects.[26] All calculations were done using the Gaussian 03 program[27] installed on the High Performance Computing cluster at the Computer Centre in The University of Hong Kong.

RESULTS AND DISCUSSION

In an Inert Solvent MeCN and a Hydrogen-Donor Solvent IPA. Figure 1 displays the fs-TA results obtained after photolysis of *m*-BPOH in MeCN. Spectra at early (before 1 ps) and late delay times are given separately to clarify the spectral changes that take place on different time scales. Upon irradiation, the ground state of *m*-BPOH is transferred to a higher excited singlet state S_n and the very early time TA spectra can be assigned to the relaxation from the S_n to S_1 state and the initial species that appears at 340 nm within 1 ps was assigned to the $S_1 \rightarrow S_n$ absorption from $(m\text{-BPOH})^1$ (the singlet excited state of *m*-BPOH). The time constant for internal conversion (IC) from S_n to S_1 is within the instrument response time, and thus, it will not be discussed further. Subsequently, a second species with a broad band around 530 nm is formed. The coincidence between the decay time constant of $(m\text{-BPOH})^1$ (8 ps) and the growth time constant of the second species (8.5 ps) indicates that the second species was produced from $(m\text{-BPOH})^1$. This transformation time is similar to the value of the intersystem crossing (ISC) time constant of BP (9,[28] 9.6,[29] and 10.6 ps[30]) in MeCN. Spectra at later delay times resemble those obtained from nanosecond laser flash photolysis (Figure 1c) spectra recorded for *m*-BPOH in MeCN. Time evolution analysis of the absorbance at 325 nm of *m*-BPOH in MeCN under open air and oxygen-saturated conditions were performed, and these results are given in Figure 2S, Supporting Information. The observed quenching by oxygen suggests that the species observed in ns-TA is a triplet species in nature. Also, the triplet excited state of *m*-BPOH (denoted by $(m\text{-BPOH})^3$ hereafter) was detected in the ns-TR^3 spectra of *m*-BPOH in MeCN.[13] Therefore, the transformation observed by fs-TA in MeCN was assigned to the ISC process from $(m\text{-BPOH})^1$ to $(m\text{-BPOH})^3$, and the fully developed spectra in Figure 1b are assigned to the $T_1 \rightarrow T_n$ absorption.

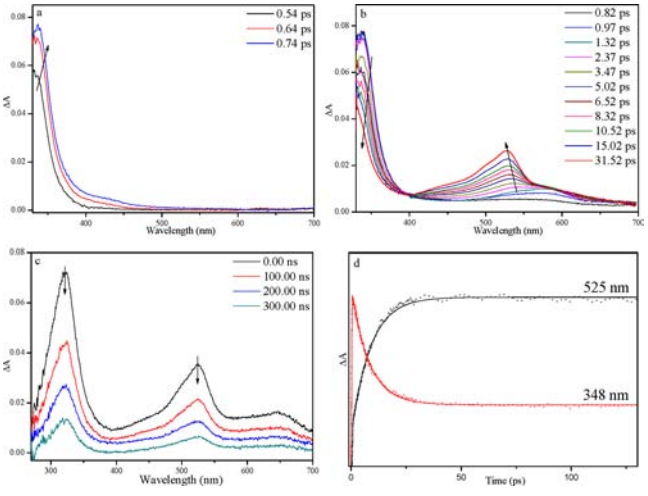

Figure 1. (a and b) Femtosecond-TA and (c) ns-TA spectra of *m*-BPOH in MeCN acquired after 266 nm irradiation of the sample. (d) Spectral temporal dependences observed at 348 and 525 nm in MeCN detected by the fs-TA experiment.

Figure 2 depicts the fs-TA and ns-TA results obtained for 2-HEAQ in MeCN. As a close relative to BP, the broader spectral profiles and red-shifted maximum of the band in Figure 2a are also associated with the IC process from a higher excited S_n to S_1. Therefore, the very early time TA spectra can be assigned to the transformation from S_n to S_1, and the species appearing at 381 nm within 1 ps was assigned to the $S_1 \rightarrow S_n$ absorption from S_1. Subsequently, a second species with bands at 454 and 640 nm appears in the later delay time fs-TA spectra, and this

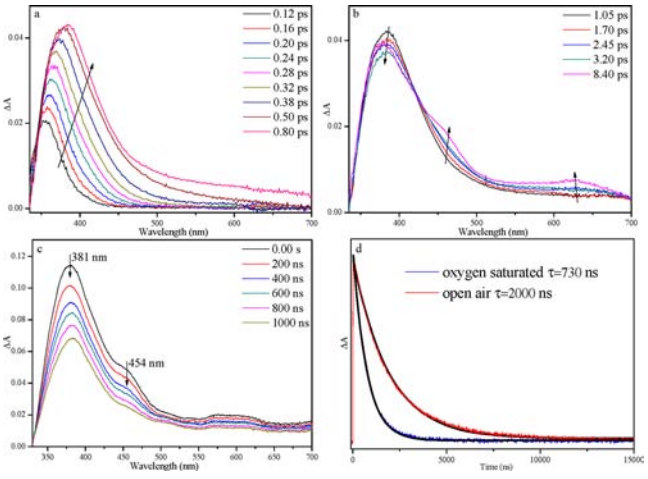

Figure 2. (a and b) Femtosecond-TA and (c) ns-TA spectra of 2-HEAQ in MeCN acquired after 266 nm excitation. (d) Time evolution with initial growth followed by decay of ΔA monitored at 380 nm under open and oxygen-saturated conditions.

dx.doi.org/10.1021/ja304441n | J. Am. Chem. Soc. 2012, 134, 14858−14868

species was also detected by ns-TA spectra under the same experimental conditions. In the presence of a higher oxygen concentration in solution, this species has a reduced lifetime in the ns-TA spectra, suggesting this species is triplet in nature. The triplet excited states of 9,10-AQ and 2-(hydroxymethyl) anthraquinone were reported to have an intense 380 nm absorption and a minor absorption at 660 nm in MeCN, which are similar to the observation in Figure 2.[3e,10]

Therefore, the species observed in ns-TA and later time delay fs-TA spectra is assigned to the triplet excited state of 2-HEAQ (denoted as $(2\text{-HEAQ})^3$), and the transformation observed by fs-TA in MeCN is attributed to the ISC to the lowest triplet excited state.

Figure 3S, Supporting Information, displays the ns-TR^3 spectra of 2-HEAQ in MeCN, and mainly one species attributed to $(2\text{-HEAQ})^3$ was observed. Comparison of the predicted Raman spectrum from the DFT calculations for $(2\text{-HEAQ})^3$ and the 5 ns time delay experimental TR^3 spectrum (Figure 4S, Supporting Information) shows that the calculated normal Raman spectrum displays reasonably good agreement with the TR^3 spectrum and confirms that the species is $(2\text{-HEAQ})^3$. Observation of $(2\text{-HEAQ})^3$ by fs-TA, ns-TA, and ns-TR^3 experiments demonstrates that 2-HEAQ can transfer to the triplet excited state very fast and efficiently so some photochemical reactions may be able to compete with photophysical radiative and radiationless decay pathways. Optimized structures for the singlet ground state of 2-HEAQ and $(2\text{-HEAQ})^3$ (Figure 5S, Supporting Information) indicate that $(2\text{-HEAQ})^3$ has a significantly longer C═O bond length (1.30 Å) in the AQ group compared to that of the singlet ground state of 2-HEAQ (1.22 Å), and the bond length of the methylene C−H bond does not exhibit an obvious change in both structures. Thus, $(2\text{-HEAQ})^3$ is highly polarized with an enhanced electron density on the central ring of the AQ moiety and a lower electron density on the benzene ring with the attached hydroxymethyl group, suggesting an excited state electron migration from the aromatic ring of the benzyl alcohol to the AQ group.[3f]

The traditional photoreduction reaction for aryl ketones was also examined using ns-TA and ns-TR^3 techniques for 2-HEAQ in the strong hydrogen-donor solvent IPA. Photoreduction of AQ was first reported by Wilkinson and co-workers,[31] and more recently, the mechanism was investigated in detail using time-resolved transient spectroscopy by Görner.[10] In the IPA solution, the transient species absorbs at 383 and 430 nm, bleaches at 320 nm in the ns-TA spectra, and can be fitted with a first-order kinetics decay (Figure 3). The ns-EM experiment of 2-HEAQ in IPA (Figure 6S, Supporting Information) shows that a transient species is generated and emits ~320 nm. On the other hand, it has been reported that the semi-anthraquinone radical is formed by a hydrogen abstraction reaction of the triplet excited state of the AQ moiety from alcohols and can further abstract a hydrogen atom to produce dihydroxyanthracene, which has a strong fluorescence emission around 320 nm with a lifetime of tens of nanoseconds.[10,31] Therefore, the long-lived transient species detected here indicates there is formation of 2-(1-hydroxyethyl) 9,10-dihydroxyanthracene. The species absorbed at 383 and 430 nm is tentatively attributed to the semianthraquinone radical, and the negative signal around 320 nm in Figure 3 has contributions from both the dihydroxyanthracene species and the ground state bleaching of 2-HEAQ (see Figure 1S, Supporting Information). To gain structural information for

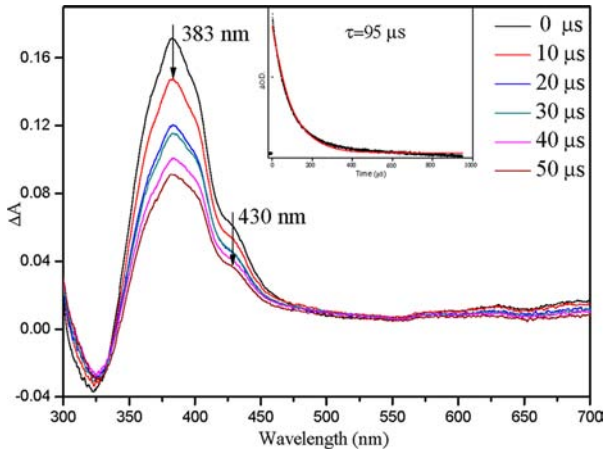

Figure 3. Nanosecond-TA spectra of 2-HEAQ in IPA after 266 nm irradiation. (Inset) Time evolution with initial growth followed by decay of ΔA monitored at 380 nm.

the reactive intermediates, the ns-TR^3 experiment was performed for 2-HEAQ in IPA.

Examination of Figure 4 suggests that a species with its most intense Raman bands at 1545, 1570, and 1612 cm^{-1} overlaps

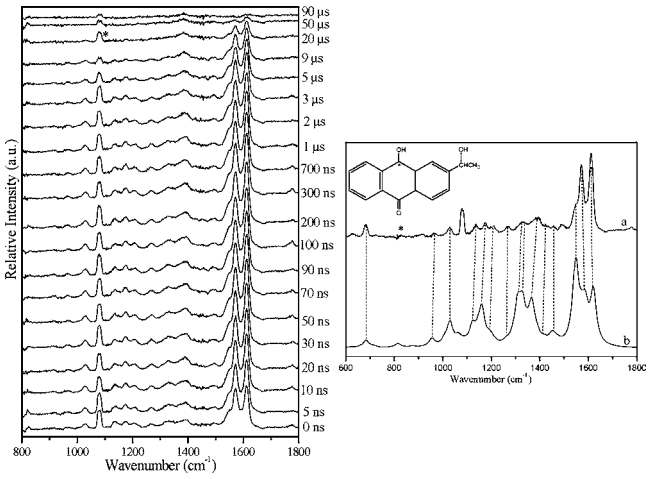

Figure 4. (Left) Nanosecond-TR^3 spectra of 2-HEAQ in IPA obtained at various time delays indicated next to the spectra. (Right) Comparison of (a) the 90 ns experimental Raman spectrum to (b) the calculated ketyl radical species of 2-HEAQ.

with the Raman bands of $(2\text{-HEAQ})^3$ at 1570 cm^{-1}. As the delay time between the pump and the probe lasers increases, the 1612/1570 cm^{-1} band intensity ratio increased from ca. 1.1 at 0 ns to 1.3 at 20 ns and remained constant thereafter, and the spectral profile did not change until it diminished after 90 μs. On the basis of previous studies of AQs, the new species is generated from photoreduction of $(2\text{-HEAQ})^3$ by the hydrogen-atom abstraction reaction with the IPA solvent that makes the semianthraquinone radical species having absorption bands at 383 and 430 nm in the ns-TA spectra. The calculated Raman spectrum of the ketyl radical species of 2-HEAQ was compared with the experimental spectrum obtained at 200 ns (Figure 4). The main Raman bands of the ketyl radical species of 2-HEAQ are from C═O and C−C vibrations. Two types of T_1 states, with mainly $n\pi^*$ or $\pi\pi^*$ character, respectively, have been identified to be responsible for the differences in the photophysical and photochemical behavior of aromatic carbon-

dx.doi.org/10.1021/ja304441n | J. Am. Chem. Soc. 2012, 134, 14858−14868

yl triplets. The nπ^* T_1 species exhibits a high efficiency for the hydrogen abstraction reaction, whereas a triplet state with $\pi\pi^*$ character typically has low reactivity for hydrogen abstraction.[32] Thus, the efficient photoreduction reaction of 2-HEAQ in IPA suggests that nπ^* is the main configuration for $(2\text{-HEAQ})^3$ in IPA.

In Neutral, Acid, and Alkaline Aqueous Solutions. To elucidate the photoredox reaction mechanism and gain direct information about the reactive intermediates involved, fs-TA, ns-TA, and ns-TR^3 experiments were conducted for 2-HEAQ in aqueous solutions with varying pH values.

On the basis of the fs-TA spectra obtained in MeCN, the initial spectral profile changes observed in the fs-TA spectra acquired in MeCN:H_2O (1:1, pH 6−7) solution (Figure 5)

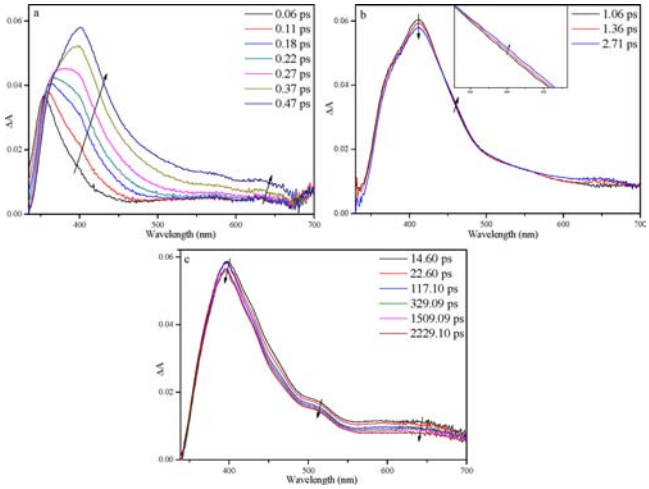

Figure 5. Femtosecond-TA spectra of 2-HEAQ in MeCN:H_2O (1:1, pH 6−7) under irradiation of 266 nm.

from 360 to 395 nm has most of its contribution from the IC process to form $(2\text{-HEAQ})^1$. In addition, the decrease of the band around 395 nm can be attributed to ISC that produces $(2\text{-HEAQ})^3$. After formation of $(2\text{-HEAQ})^3$ a new species (denoted as **X**) that was not detected by the fs-TA spectra in MeCN appeared with a characteristic band at 510 nm and a weak broad band at the longer wavelength region around 650 nm within 10 ps and then started to decay. fs-TA spectra obtained in pH 2 MeCN:H_2O (1:1) solution (data not given) exhibited great similarity with Figure 5. Assignment of thespecies **X** will be discussed in a later section with the help of a comparison of the fs-TA spectra acquired in aqueous solutions with varying pH values.

Figure 6 shows the ns-TA spectra acquired after photolysis of 2-HEAQ in neutral aqueous solutions with different water concentrations. The obviously different transient spectra profile from that seen in IPA indicates that rather than the photoreduction reaction observed in IPA, a different photochemical reaction takes place in water-containing solutions. Two species were detected in the lower water concentration solution (MeCN:H_2O, 9:1). The first species A has shoulder bands at 388 and 457 nm, and the second species B appearing at later times absorbs at 392 nm. In a medium water concentration solution (MeCN:H_2O, 1:1), species B was observed upon irradiation and after several thousands of nanoseconds a new species C appeared with bands around 370 and 480 nm. When the water concentration was increased to 90%, the spectra resembled those acquired at medium water

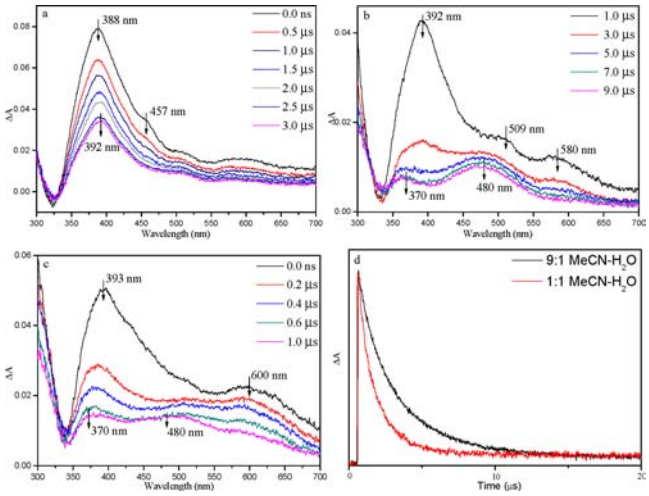

Figure 6. Nanosecond-TA spectra of 2-HEAQ after 266 nm photolysis in (a) MeCN:H_2O (9:1, pH 6−7), (b) MeCN:H_2O (1:1, pH 6−7), and (c) MeCN:H_2O (1:9, pH 6−7) mixed solutions. (d) Normalized transient decays of 2-HEAQ in (black) MeCN:H_2O (9:1, pH 6−7) and (red) MeCN:H_2O (1:1, pH 6−7) monitored at 390 nm.

concentration, while the lifetime of the species B was shorter and species C appeared more quickly after only 200 ns. Figure 6d depicts the temporal evolution of the absorbance at 390 nm observed in low and medium water concentrations, and the signal decay at this wavelength was too fast to probe accurately at higher water concentration (MeCN:H_2O, 1:9). Obviously, decay of this signal accelerated as the water concentration increased. These results reveal that water is essential for the photochemical reaction of 2-HEAQ to take place efficiently. Therefore, the new photochemical reaction appears hindered in lower water concentration solutions and is promoted in higher water concentration solutions, and the species observed by ns-TA were generated through the following route

$$A \rightarrow B \rightarrow C$$

Combining the ns-TA and fs-TA results obtained under the same conditions, the transient species A observed in neutral aqueous solutions can be assigned to $(2\text{-HEAQ})^3$. Species B, which can be quenched by water, has a similar spectrum profile with species **X** observed in the fs-TA spectra in the same solution, suggesting they may be the same species in nature or have similar structure and electronic character. The long lifetime of C suggests it may be a ground state species which could be the final product generated from the photoredox reaction under ns-TA experimental conditions. The resemblance of its spectra profile to the dihydroxyanthracene UV−vis spectrum suggests that transient C may be due to species 2-formyl-9,10-dihydroxyanthracene. It is also important to note that a bleaching band was observed around 320 nm in the low water concentration solution similar to the one detected in IPA solution (this was not observed in the medium and high water concentration solutions), and this will be discussed later. Since the absorption spectra are broad and do not reveal much structural information about the transient species observed, ns-TR^3 experiments were performed to help better characterize and clearly identify the transient species.

In agreement with the fs-TA and ns-TA results, the ns-TR^3 spectra of 2-HEAQ in neutral (Figure 7S, Supporting Information) and pH = 2 (Figure 7) aqueous solutions exhibit great similarity with each other and are very different from

dx.doi.org/10.1021/ja304441n | J. Am. Chem. Soc. 2012, 134, 14858−14868

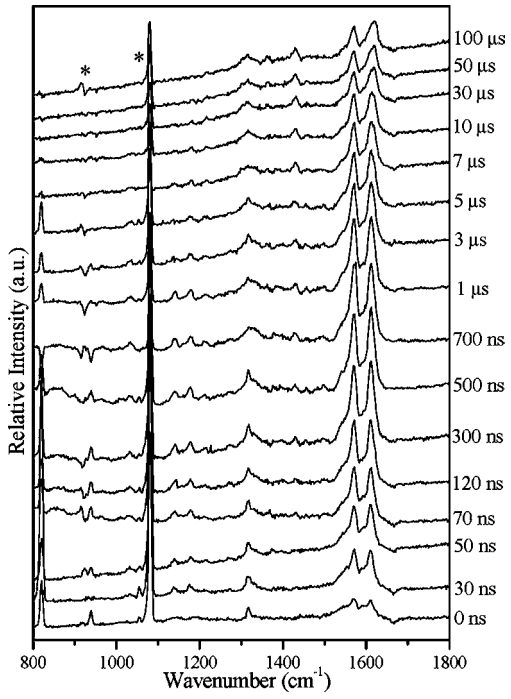

Figure 7. Nanosecond-TR^3 spectra of 2-HEAQ in aqueous solution (MeCN:H_2O, 1:1) at pH 2 obtained at various time delays indicated next to the spectra. Asterisk (*) marks regions affected by solvent subtraction artifacts and/or stray light.

those obtained in IPA solution. The same species with its Raman bands at 1140, 1177, 1212, 1318, 1570, and 1612 cm^{-1} was produced upon irradiation and existed for a relatively long time in the two solutions. Closer examination reveals this species had a higher intensity in the acid solution than that in the neutral solution upon irradiation. At later times (10 μs and afterward) the Raman bands of 1140 and 1177 cm^{-1} disappeared and the 1612 cm^{-1} peak shifted to 1618 cm^{-1} and the intensity ratio of the Raman bands 1570/1612 cm^{-1}changed from ~1 to >1 in acid solutions; this suggests generation of a new species that takes place at a slower rate in neutral solution. The Raman signal of (2-HEAQ)^3 was also not detected in the spectra displayed in Figures 7 and 7S, Supporting Information, indicating that the main species detected by the ns-TR^3 spectra in both neutral and moderate acid (pH = 2) aqueous solutions is mainly the transient species B observed in the ns-TA spectra under the same conditions.

Oxygen quenching ns-TR^3 experiments were conducted, and these results are shown in Figure 8S, Supporting Information. The Raman bands of species B at 1570 and 1612 cm^{-1} in the presence and absence of oxygen were fitted with a Lorentzian band shape; it was found that the yield of this species was reduced by oxygen, while its decay rate was not affected. This suggests species B is a ground state species that is generated from the triplet excited state. Hence, the experimental Raman spectra at 90 ns and 20 μs were, respectively, compared with the calculated Raman spectra of the transient species **2** (see Schemes 2 and 3) and the final product 2-acetyl 9,10-anthraquinone (see Figure 9S, Supporting Information). The similarity between the calculated spectra with the respective experimental spectra supports the tentative assignment of the intermediate species and confirms the occurrence of the photoredox reaction of 2-HEAQ in neutral and moderate acid aqueous solution. Detection of 2-(1-hydroxyethyl) 9,10-dihydroxyanthracene (transient C observed in ns-TA spectra) is probably due to this species not being oxidized to the final product yet since the ns-TA experiments used a sample contained in a closed cell and a short data collection time that limited sample exposure to air after a fresh sample was prepared for use in these experiments. On the other hand, the ns-TR^3 experiments need a much longer data collection time and use of a flowing liquid stream of sample that had much greater exposure to oxygen in the air; this appears to have oxidized 2-(1-hydroxyethyl) 9,10-dihydroxyanthracene to the final product 2-acetyl 9,10-anthraquinone detected in these experiments at longer times (refer to the Supporting Information for a more detailed description of the experimental conditions).

The role of water was further elucidated by ns-TR^3 experiments performed in neutral aqueous solutions with varying water concentrations. In a low water concentration (MeCN:H_2O, 9:1) (Figure 10S, Supporting Information), the Raman signal of (2-HEAQ)^3 was observed at early delay times (within 20 ns). Then the same transient species **2** was generated with an obviously lower intensity compared with the results obtained in a medium water concentration (MeCN:-H_2O, 1:1). This indicates that in a certain range the efficiency of the photoredox reaction was improved when increasing the water concentration. ss-TR^3 experiments were also conducted in a neutral deuterium mixed solution (MeCN:D_2O, 1:1) (Figure 11S, Supporting Information). The photoredox reaction proceeded much more slowly than in the water solution (MeCN:H_2O, 1:1) at neutral pH, (2-HEAQ)^3 was detected within 50 ns, and the lifetime of the species **2** was estimated to be 600 ns in MeCN:D_2O (1:1) solution and 300 ns in MeCN:H_2O (1:1). The observed k_H/k_D = 2 indicates there is involvement of water in the reaction. These experimental results from ns-TA and ns-TR^3 experiments unravel three things. First, the photoredox reaction mainly proceeded via the reactive triplet excited state species (2-HEAQ)^3. Second, the photoredox reaction was mediated and catalyzed by water and had faster kinetics in a moderate acidic solution than in a neutral aqueous solution. Third, since even in the medium water concentration solution (MeCN:H_2O, 1:1) water molecules (17 mM) far outnumber the substrate 2-HEAQ (0.5 mM) and are adequate to promote the photoredox reaction. On the other hand, extensive investigations on aromatic carbonyl compounds reveal that increasing the H-bonding strength or polarity of the solvent stabilizes $\pi\pi^*$ states, whereas these effects destabilize the $n\pi^*$ state at the same time.[33−42] Therefore, we propose that the photoredox reaction of 2-HEAQ in aqueous solutions proceeds via a species with $\pi\pi^*$ character, which is different from the photoreduction reaction in IPA that takes place via a species with mainly $n\pi^*$ character. The absence of water may result in a shift of the triplet state to have more $n\pi^*$ character, which is favorable for the hydrogen abstraction associated with the photoreduction reaction. This is consistent with the observation of a fluorescent species in the lower water concentration solutions (MeCN:-H_2O, 9:1), which may be generated from the photoreduction reaction similar to what was observed in the IPA solution. The photoreduction reaction of 2-HEAQ with the MeCN cosolvent could take place and become a competing reaction of the photoredox reaction in lower water concentrations with a neutral pH value. The C═O vibrational modes are around 1600 cm^{-1} in both the calculated Raman spectrum and the experimental spectrum in the aqueous solutions. This provides further support that the photoredox reaction occurs from a

dx.doi.org/10.1021/ja304441n | J. Am. Chem. Soc. 2012, 134, 14858−14868

species with $\pi\pi^*$ character. Photoreduction of aromatic ketones typically proceeds via the $n\pi^*$ triplet state, whereas the photoredox reaction most likely proceeds via a species with some $\pi\pi^*$ triplet character. It has been reported that the $\pi\pi^*$ configuration is preferred in rich water concentration solutions.[33−42]

Femtosecond-TA and ns-TR^3 experiments were conducted in moderate basic mixed aqueous solutions at pH 10. Species **X** appeared in the fs-TA spectra, and the same Raman signals obtained in neutral and moderate acid aqueous solution at pH = 2 were observed but with noticeably lower intensities. These results suggest that the photoredox reaction can still take place but with obviously lower yield. In other words, the photoredox reaction is not preferred in moderate basic aqueous solution, where deprotonation of the C−H bond on the benzyl CH_2OH moiety would be more efficient.

In Strong Basic (pH = 13) and Strong Acidic (pH = 0) Aqueous Solutions. Having characterized the photoredox reaction in neutral, moderate acid, and basic aqueous solutions, fs-TA, ns-TA, and ns-TR^3 experiments were next conducted for 2-HEAQ in pH = 13 and 0 aqueous solutions to investigate whether the same reaction will take place or even be facilitated by higher concentrations of hydroxide ions and protons.

When the pH value was increased to pH 13 only the ISC transformation and (2-HEAQ)^3 was detected in the fs-TA and ns-TR^3 spectra (Figures 12S and 13S, Supporting Information), respectively. This indicates 2-HEAQ experiences an unproductive pathway in strong basic conditions, and the reactivity for 2-HEAQ in this environment will not be discussed further here. Since protonation still takes place (albeit with a lower yield compared to neutral pH) at pH 10 and does not take place at all at pH 13, it is possible that the pK_a of the carbonyl oxygen of the excited state of 2-HEAQ is close to 10. Resonance Raman spectra for *m*-BPOH and 2-HEAQ obtained in acidic aqueous solution at pH 0 were identical with those obtained in a neutral aqueous solution (data not given), suggesting that the carbonyl oxygen in the ground state was not protonated under this condition. Therefore, the species irradiated in the pH = 0 mixtures were still the normal form for both *m*-BPOH and 2-HEAQ.

Figure 8 depicts the fs-TA spectra of *m*-BPOH obtained after photolysis in pH = 0 MeCN−H_2O solution. The spectral profile exhibits great similarity with that obtained in MeCN, and the ISC process was also observed in this solution. Closer examination of the spectra reveals that the isosbestic point red shifted to 380 nm, which suggests that the long-wavelength band broadened more than in MeCN. (*m*-BPOH)^3 began to decay after 30 ps (Figure 8c), and fast consumption of (*m*-BPOH)^3 suggested that it was the precursor for a new reaction. ns-TR^3 studies revealed that the photohydration reaction reported by Wirz for BP was also the predominant reaction for *m*-BPOH in pH = 0 aqueous solution, and photohydration takes place with an initial protonation reaction of the carbonyl oxygen. On the other hand, it is well established that aromatic ketones become stronger bases upon electronic excitation.[43] Hence, the decay of (*m*-BPOH)^3 detected by fs-TA under the same conditions probably resulted from protonation of (*m*-BPOH)^3 with formation of the protonated species of (*m*-BPOH)^3. The fs-TA spectral profile of *m*-BPOH obtained in a mixed aqueous solution with pH 2 displayed great similarity with that obtained in the pH 0 acidic aqueous solution.

Hence, the photoredox reaction studied in pH = 2 aqueous solutions also takes place via protonation of (*m*-BPOH)^3 first.

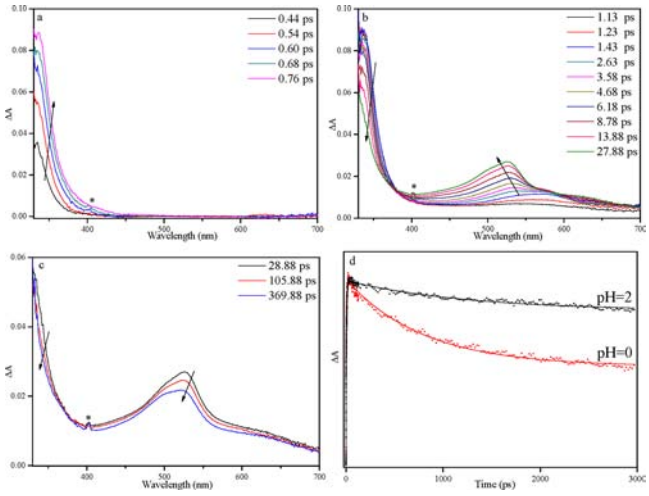

Figure 8. (a−c) Femtosecond-TA spectra of *m*-BPOH in pH = 0 H_2O−MeCN solution (1:1) at different time regions recorded after 266 nm excitation. Asterisk (*) marks regions affected by subtracted scattered light at 400 nm. (d) Normalized transient absorption dynamics of (*m*-BPOH)^3 recorded at 545 nm in H_2O−MeCN (1:1) mixtures at pH = 2 and 0.

This is consistent with the fact that the photoredox reaction of *m*-BPOH competes with the photohydration reaction within the pH region from 4 to 0. The lifetime of (*m*-BPOH)^3 in the pH = 0 mixed aqueous solution can be fit by a two-exponential function with a growth time constant of 5 ps and a decay time constant of 792 ps. In the pH = 2 mixed solution, the growth time constant was similar (5.6 ps) but there was a longer decay constant of 1275 ps for (*m*-BPOH)^3. This proton concentration dependence decay dynamics confirms that (*m*-BPOH)^3 is a reactive precursor to the photochemistry events observed previously in water-containing solutions and validates that protonation of the carbonyl oxygen is the initial process for the photoredox reaction of *m*-BPOH on the other hand. These results are also consistent with previous studies reporting that the carbonyl oxygen was protonated under pH 0 aqueous solutions for the triplet excited state of BP[44] and *S*-ketoprofen.[45] fs-TA spectra of 2-HEAQ obtained in pH = 0 mixed aqueous solution bear great resemblance to those obtained in neutral and pH = 2 aqueous solutions (Figure 5), and species **X** was also observed after formation of (2-HEAQ)^3. Similarly, species **X** that absorbed around 510 nm in the fs-TA spectra obtained in pH = 0 as well as in neutral and pH = 2 aqueous conditions can be assigned to the carbonyl-protonated (2-HEAQ)^3, denoted as the transient species **1** in Scheme 3. It is noted that the UV−vis spectra profile for species **X** (observed in fs-TA) bears some similarity with that of species B observed in the ns-TA spectra (Figure 6), while they were assigned as different species, transient species **1** and **2**. Further support for such assignments comes from the TD-DFT calculations (Figure 14S, Supporting Information), showing that simulated UV−vis absorption spectra of species **1** and **2** exhibited reasonable resemblance with the corresponding experimental spectra for species **X** and B.

Two species were detected by ns-TR^3 experiments (Figure 9) done in the pH = 0 aqueous solutions (MeCN:H_2O, 1:1). The first species with its intense Raman bands at 1472, 1505, 1570, and 1602 cm^{-1} appeared upon irradiation and decayed within 10 ns, and then the second species with bands at 1570 and 1618 cm^{-1} was generated and with a relatively long lifetime.

dx.doi.org/10.1021/ja304441n | J. Am. Chem. Soc. 2012, 134, 14858−14868

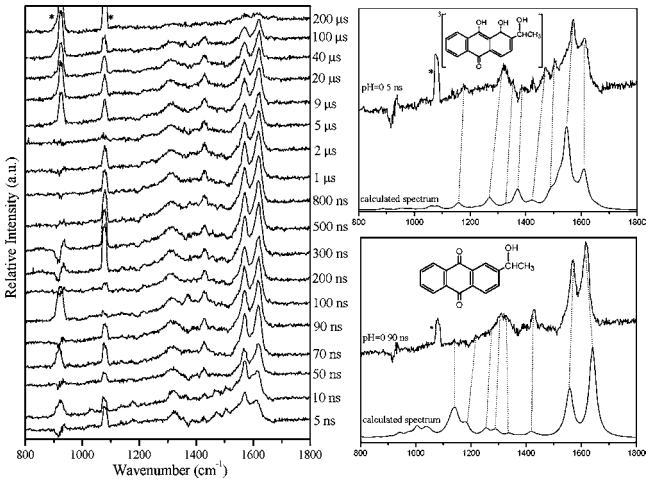

Figure 9. (Left) Nanosecond-TR^3 spectra of 2-HEAQ in pH = 0 (MeCN:H_2O, 1:1) solution obtained at various time delays indicated next to the spectra. (Right) Comparison of (top) ns-TR^3 at 5 ns with the calculated structure of the triplet state trihydroxyl−carbonyl and (bottom) ns-TR^3 at 90 ns with the calculated Raman spectrum of the singlet 2-HEAQ.

The obviously different ns-TR^3 (Figure 9) and ns-TA (Figure 15S, Supporting Information) results for 2-HEAQ in a pH = 0 aqueous solution (MeCN:H_2O, 1:1) from those obtained in neutral and moderate acidic and basic aqueous solutions indicates that the photoredox reaction goes away and 2-HEAQ has access to an alternative reaction route in more acidic solutions after formation of the triplet carbonyl-protonated (2-HEAQ)^3. Previous studies showed that the photohydration reaction reached its maximum yield for BP and was also the predominant reaction for *m*-BPOH in pH = 0 aqueous solutions,[13,44] while the photoredox reaction was not obvious for *m*-BPOH in very high acidic aqueous solutions at pH 0 as reported in Wan and co-workers product analysis work done under similar conditions.[3g] Therefore, photohydration of 2-HEAQ was proposed to be the major reaction observed under the same conditions, and the photohydration reaction mechanism is depicted in Scheme 4 based on Wirz's study

Scheme 4. Proposed Photohydration Reaction Mechanism for 2-HEAQ in Acid Aqueous Solution Based on the Study of BP by Wirz and Co-workers[44]

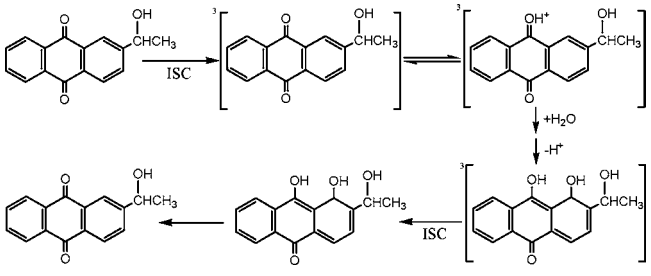

on BP.[44] It is noted that photohydration takes place at both the ortho and the meta positions and the ortho hydration would yield a transient with a longer lifetime.[44,46] Hence, we mainly take ortho hydration into consideration for 2-HEAQ because of its long lifetime, although meta hydration may also contribute to the signal. An oxygen quenching experiment (Figure 16S, Supporting Information) showed that the lifetime of the second species was not affected while its yield was reduced, and this suggests that the second species is a singlet species in nature and produced via a triplet character species. The first species observed in the pH = 0 aqueous solution by ns-TR^3 was assigned to the trihydroxyl-triplet intermediate. Comparison between the experimental and the calculated Raman bands for the two species (Figure 9, right) showed reasonable similarity and supported the attribution that the photohydration reaction is the predominant reaction in pH = 0 aqueous solutions for 2-HEAQ, and no obvious Raman signal for the photoredox reaction was detected.

Since the photohydration reaction also proceeds via the protonated excited state species of 2-HEAQ, the absence of the photoredox reaction in pH = 0 indicates that the deprotonation reaction is a requisite step for the photoredox reaction. A plausible explanation is that the pK_a of the methylene C−H that is deprotonated is close to 2, and thus, deprotonation is not favored at pH 0. On the other hand, incorporating detection of the carbonyl-protonated 2-HEAQ after the ISC process by the fs-TA spectra and the fact that the photoredox reaction takes place at a faster rate in a pH = 2 aqueous solution than in a neutral aqueous solution, it is more plausible to propose that the protonation process at the AQ carbonyl oxygen should be the first step and rate-determining process for the photoredox reaction of 2-HEAQ. Therefore, we propose that the photoredox reaction takes place via the mechanism depicted in Scheme 3 rather than the one given in Scheme 2. Water plays an essential role for the photoredox reaction to stabilize the initial excited state and the ionic intermediates generated, as well as to provide protons in the reaction mechanism.

DFT Calculations for the Photoredox Reaction. To better understand the photoredox reaction of 2-HEAQ in aqueous solutions, DFT calculations were utilized to examine the activation barrier. Computations were performed at the (U) B3LYP/6-31G* level of theory. Figures 10 and 11 show the

Figure 10. Optimized geometries of RC_1, TS_1, and PC_1 obtained from (U)B3LYP/6-31G* calculations for the protonation reaction of (2-HEAQ)^3 with H_2O. Selected interatomic distances (Angstroms) are labeled.

optimized structures of the reactant complex (RCn), transient state (TSn), and product complex (PCn), where n represents the sequence of the reaction steps for the photoredox reaction

Figure 11. Optimized geometries of RC_2, TS_2, and PC_2 obtained from (U)B3LYP/6-31G* calculations for deprotonation reactions after protonation of (2-HEAQ)^3 with H_2O. Selected interatomic distances (Angstroms) are labeled.

dx.doi.org/10.1021/ja304441n | J. Am. Chem. Soc. 2012, 134, 14858−14868

of (2-HEAQ)^3. The photoredox reaction of 2-HEAQ with water was confirmed to proceed via two dynamical steps, whereby water donates a proton to the 2-HEAQ carbonyl oxygen through TS_1 in the first step. This reaction is initiated through hydrogen bonding between the proton donor and acceptor as indicated by the distance change between the O atom in 2-HEAQ and the H atom from water from 2.14 to 1.16 Å. (Figure 10). As the reaction goes from TS_1 to PC_1, the H−O bond of the water molecule is completely cleaved, protonating the carbonyl oxygen in 2-HEAQ. Thus, the carbonyl oxygen is protonated first to generate the protonated intermediate. In the second step, deprotonation occurs at the side chain via TS_2 and the bond length of the C−H bond elongates from 1.096 to 1.157 Å, resulting in deprotonation and cleavage of the C−H bond. The final product is then formed by those two steps.

The relative energy profile following the protonation and deprotonation reactions obtained from the transition state calculations is displayed in Figure 12. Inspection of Figure 12

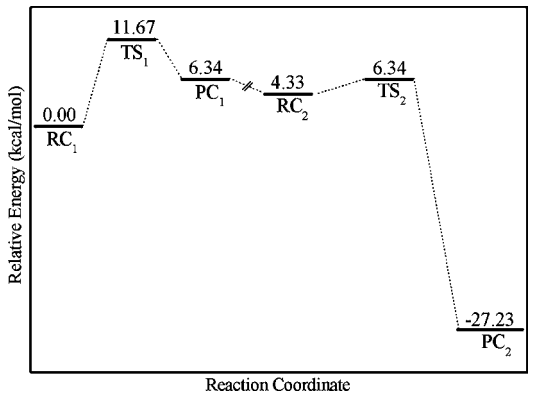

Figure 12. Reactive energy profile obtained from (U)B3LYP/6-31G* calculations for the photoredox reaction of (2-HEAQ)^3 following the initial protonation reaction and subsequent deprotonation route.

indicates that the initial protonation step experiences an activation energy barrier of 11.7 kcal mol^{-1}, and the subsequent reaction overcomes a 2.0 kcal mol^{-1} activation energy barrier. Clearly, the first step is the rate-determining reaction. This is consistent with the experimental result that a higher efficiency of the photoredox reaction was observed in moderate acid aqueous solution than in a neutral aqueous solution. Furthermore, the relatively lower energy of the final product complex (PC) compared to that of the reactant complex and transition states suggests the photoredox reaction of (2-HEAQ)^3 is exothermic by −27.2 kcal mol^{-1}.

CONCLUSION

Using fs-TA, ns-TA, and ns-TR^3 spectroscopic techniques as well as DFT calculations, the present article reports an investigation of the photophysical and photochemical reactions of 2-HEAQ in MeCN, IPA, and neutral, acid, and basic aqueous solutions. The ISC process of 2-HEAQ took place in MeCN to produce (2-HEAQ)^3, which underwent mainly the photoreduction reaction in an IPA solvent. A novel photoredox reaction takes place via an initial protonation process of the AQ group that is followed by deprotonation of the methylene C−H bond in aqueous solutions within a pH range from 2 to 10. In stronger acidic aqueous condition of pH = 0, the photohydration reaction becomes the major reaction. Only ISC appears to occur with unreactive processes in strong basic solutions (pH = 12). The photophysical and photochemical characteristics of 2-HEAQ embodies noticeable similarity with that of *m*-BPOH, with the exception that 2-HEAQ undergoes the photoredox reaction in neutral aqueous solution while *m*-BPOH does not exhibit an obvious photoredox reaction under the same reaction condition. This can be attributed to the stronger basicity in the excited state of the carbonyl oxygen of the AQ system than in the BP group. Combing the fs-TA, ns-TA, ns-TR^3 results and the results from DFT calculations, a proposed reaction mechanism of the photoredox reaction of 2-HEAQ in aqueous solution is displayed in Scheme 5 with all letters and numbers used in the text for the key intermediates given below the chemical structures used in the text.

Scheme 5. Proposed Reaction Mechanism of the Photoredox Reaction of 2-HEAQ in Aqueous Solution[a]

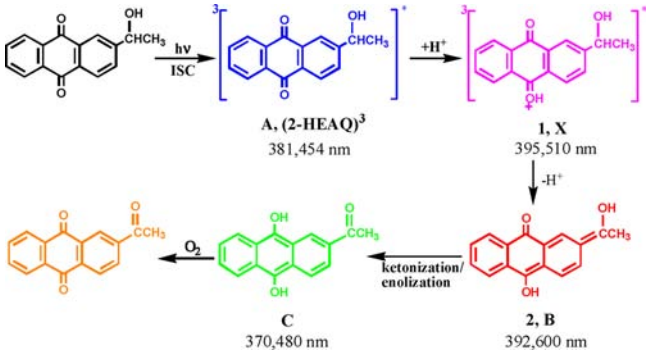

[a]Letters and numbers below the structures are the corresponding labels used in the text. Absorbance for the transient species detected from fs-TA and/or ns-TA spectra are given.

The AQ system by an initial excited state electron migration from the aromatic ring of the benzyl alcohol to the AQ followed or coupled by trapping with solvent protons sheds insights on the photoactivation of distal functional groups mediated by phenylene spacers. These are unprecedented examples of how two functional groups can undergo "coupled" photochemistry mediated by a conjugated π system. The photoredox, photoreduction, and photohydration reactions observed for 2-HEAQ in aqueous solutions suggest that the reaction mechanism(s) for photodeprotection reactions utilizing 2-HEAQ as the photoremovable protecting group need further work to better understand how deprotection takes place in this platform of molecules under varying aqueous conditions. Last but not least, this kind of novel and efficient photoredox reaction has promising application as a new photochemical synthetic method to promote coupled reactions for distal functional groups.

ASSOCIATED CONTENT

Supporting Information

Detailed descriptions of the femtosecond time-resolved transient absorption, nanosecond time-resolved transient absorption, and nanosecond time-resolved resonance Raman experimental instrumentation and methods; additional spectra obtained under varying conditions; tables of excited state energies and oscillator strengths from TD-DFT calculations for the interested transient species; Cartesian coordinates, total energies, and vibrational zero-point energies for the optimized geometry from (U)B3LYP/6-311G** calculations for the compounds and intermediates considered in this paper. This

dx.doi.org/10.1021/ja304441n | J. Am. Chem. Soc. 2012, 134, 14858−14868

material is available free of charge via the Internet at http://pubs.acs.org.

AUTHOR INFORMATION

Corresponding Author

E-mail: phillips@hku.hk

Notes

The authors declare no competing financial interest.

ACKNOWLEDGMENTS

This research was supported by grants from the Research Grants Council of Hong Kong (HKU 7048/11P) to D.L.P. The Grants Committee Areas of Excellence Scheme (AoE/P-03/08) and Special Equipment Grant (SEG HKU/07) are also gratefully acknowledged. We thank Professor Peter Wan and Dr. Yunyan Hou at the University of Victoria for generously providing the sample 2-(1-hydroxyethyl) 9,10-anthraquinone (2-HEAQ) used in this study.

REFERENCES

(1) (a) Wan, P.; Yates, K. *J. Org. Chem.* **1983**, *48*, 136−138. (b) Wan, P.; Yates, K. *Can. J. Chem.* **1986**, *64*, 2076−2086.

(2) Dopp, D. In *CRC Handbook of Organic Photochemistry and Photobiology*; Horspool, W. M., Song, P.-S., Eds.; CRC Press: Boca Raton, FL, 1995; Chapter 81.

(3) (a) Lukeman, M.; Xu, M.; Wan, P. *Chem. Commun.* **2002**, *2*, 136−137. (b) Huck, L. A.; Wan, P. *Org. Lett.* **2004**, *6*, 1797−1799. (c) Devin, M.; Lukeman, M.; Dan, L.; Wan, P. *Org. Lett.* **2005**, *7*, 3387−3389. (d) Basarić, N.; Mitchell, D.; Wan, P. *Can. J. Chem.* **2007**, *85*, 561−571. (e) Hou, Y. Y.; Wan, P. *Photochem. Photobiol. Sci.* **2008**, *7*, 588−596. (f) Hou, Y.; Huck, L. A.; Wan, P. *Photochem. Photobiol. Sci.* **2009**, *8*, 1408−1415. (g) Mitchell, D. P. Doctoral dissertation, University of Victoria, 2008.

(4) Aquino, A. M.; Abelt, C. J.; Berger, K. L.; Darragh, C. M.; Kelley, S. E.; Cossette, M. V. *J. Am. Chem. Soc.* **1990**, *112*, 5819−5824.

(5) Gan, H.; Whitten, D. G. *J. Am. Chem. Soc.* **1993**, *115*, 8031−8037.

(6) Yoshihara, T.; Yamaji, M.; Itoh, T.; Nishimura, J.; Shizka, H.; Tobita, S. *J. Photochem. Photobiol. A: Chem.* **2001**, *140*, 7−13.

(7) Langhals, H.; Saulich, S. *Chem.—Eur. J.* **2002**, *8*, 5630−5643.

(8) Cho, D. W.; Kim, S. H.; Yoon, M.; Jeoung, S. C. *Chem. Phys. Lett.* **2004**, *391*, 314−320.

(9) Zhu, L.; Khairutdinov, R. F.; Cape, J. L.; Hurst, J. K. *J. Am. Chem. Soc.* **2005**, *128*, 825−835.

(10) Görner, H. *Photochem. Photobiol.* **2003**, *77*, 171−179.

(11) Kobori, Y.; Fuki, M. *J. Am. Chem. Soc.* **2011**, *133*, 16770−16773.

(12) Klan, P.; Wirz, J. *Photochemistry of Organic Compounds: From Concepts to Practice*; Wiley-Blackwell: UK, 2009; Online ISBN: 9781444300017.

(13) Ma, J.; Li, M.-D.; Phillips, D. L.; Wan, P. *J. Org. Chem.* **2011**, *76*, 3710−3719.

(14) (a) Furuta, T.; Hirayama, Y.; Iwamura, M. *Org. Lett.* **2001**, *3*, 1809−1812. (b) Furuta, T.; Torigai, H.; Sugimoto, M.; Iwamura, M. *J. Org. Chem.* **1995**, *60*, 3953−3956.

(15) Ren, M.-G.; Bi, N.-M.; Mao, M.; Song, Q.-H. *J. Photochem. Photobiol. A: Chem.* **2009**, *204*, 13−18.

(16) (a) Brinson, R. G.; Jones, P. B. *Org. Lett.* **2004**, *6*, 3767−3770. (b) Sarma, S. J.; Jones, P. B. *J. Org. Chem.* **2010**, *75*, 3806−3813. (c) Jones, P. B.; Brinson, R. G.; Sarma, S. J.; Elkazaz, S. *Org. Biomol. Chem.* **2008**, *6*, 4203−4211. (d) Brinson, R. G.; Hubbard, S. C.; Zuidema, D. R.; Jones, P. B. *J. Photochem. Photobiol. A: Chem.* **2005**, *175*, 118−128.

(17) Kochevar, I. E.; Redmond, R. W. In *Methods in Enzymology*; Abelson, J. N., Simon, M. I., Eds.; Academic Press: New York, 2000; Vol. *319*, pp 20−28.

(18) Ma, C.; Kwok, W. M.; Chan, W. S.; Du, Y.; Kan, J. T. W.; Toy, P. H.; Phillips, D. L. *J. Am. Chem. Soc.* **2006**, *128*, 2558−2570.

(19) Becke, A. D. *J. Chem. Phys.* **1993**, *98*, 5648−5652.

(20) Lee, C.; Yang, W.; Parr, R. G. *Phys. Rev. B* **1988**, *37*, 785−789.

(21) Merrick, J. P.; Moran, D.; Radom, L. *J. Phys. Chem. A* **2007**, *111*, 11683−11700.

(22) Schlegel, H. B. *J. Comput. Chem.* **1982**, *3*, 214−218.

(23) Cancès, E.; Mennucci, B.; Tomasi, J. *J. Chem. Phys.* **1997**, *107*, 3032−3041.

(24) Runge, E.; Gross, E. K. U. *Phys. Rev. Lett.* **1984**, *52*, 997−1000.

(25) O'Boyle, N. M.; Tenderholt, A. L.; Langner, K. M. *J. Comput. Chem.* **2008**, *29*, 839−845.

(26) (a) Miertus, S; Scrocco, E; Tomasi, J. *Chem. Phys.* **1981**, *55*, 117−129. (b) Amovilli, C.; Barone, V.; Cammi, R.; Cancès, E.; Cossi, M.; Mennucci, B.; Pomelli, C. S.; Tomasi, J. *Adv. Quantum Chem.* **1998**, *32*, 227−261. (c) Tomasi, J.; Mennucci, B.; Cammi, R. *Chem. Rev.* **2005**, *105*, 2999−3094.

(27) Frisch, M. J.; Trucks, G. W.; Schlegel, H. B.; Scuseria, G. E.; Robb, M. A.; Cheeseman, J. R.; Montgomery, J. A., Jr.; Vreven, T.; Kudin, K. N.; Burant, J. C.; Millam, J. M.; Iyengar, S. S.; Tomasi, J.; Barone, V.; Mennucci, B.; Cossi, M.; Scalmani, G.; Rega, N.; Petersson, G. A.; Nakatsuji, H.; Hada, M.; Ehara, M.; Toyota, K.; Fukuda, R.; Hasegawa, J.; Ishida, M.; Nakajima, T.; Honda, Y.; Kitao, O.; Nakai, H.; Klene, M.; Li, X.; Knox, J. E.; Hratchian, H. P.; Cross, J. B.; Bakken, V.; Adamo, C.; Jaramillo, J.; Gomperts, R.; Stratmann, R. E.; Yazyev, O.; Austin, A. J.; Cammi, R.; Pomelli, C.; Ochterski, J. W.; Ayala, P. Y.; Morokuma, K.; Voth, G. A.; Salvador, P.; Dannenberg, J. J.; Zakrzewski, V. G.; Dapprich, S.; Daniels, A. D.; Strain, M. C.; Farkas, O.; Malick, D. K.; Rabuck, A. D.; Raghavachari, K.; Foresman, J. B.; Ortiz, J. V.; Cui, Q.; Baboul, A. G.; Clifford, S.; Cioslowski, J.; Stefanov, B. B.; Liu, G.; Liashenko, A.; Piskorz, P.; Komaromi, I.; Martin, R. L.; Fox, D. J.; Keith, T.; Al-Laham, M. A.; Peng, C. Y.; Nanayakkara, A.; Challacombe, M.; Gill, P. M. W.; Johnson, B.; Chen, W.; Wong, M. W.; Gonzalez, C.; Pople, J. A. *Gaussian 03*; Gaussian, Inc.: Wallingford, CT, 2004.

(28) Miyasaka, H.; Morita, K.; Kamada, K.; Mataga, N. *Bull. Chem. Soc. Jpn.* **1990**, *63*, 3385−3397.

(29) Tamai, N.; Asahi, T.; Masuhara, H. *Chem. Phys. Lett.* **1992**, *198*, 413−418.

(30) Kwok, W. M.; Guan, X.; Chu, L. M.; Tang, W.; Phillips, D. L. *J. Phys. Chem. B* **2008**, *112*, 11794−11797.

(31) (a) Tickle, K.; Wilkinson, F. *Trans. Faraday Soc.* **1965**, *61*, 1981−1 990. (b) Wikinson, F. *J. Phys. Chem.* **1962**, *66*, 2569−2573.

(32) (a) Baum., E. J.; Wan, J. K. S.; Pitts, J. N. *J. Am. Chem. Soc.* **1966**, *88*, 2652−2659. (b) Yang, N. C.; Dusenbery, R. L. *J. Am. Chem. Soc.* **1968**, *90*, 5899−5900. (c) Lutz, H.; Duval, M. C.; Breheret., E.; Lindqvist, L. *J. Phys. Chem.* **1972**, *76*, 821−822. (d) Wagner, P. J.; Truman, R. J.; Scaiano, J. C. *J. Am. Chem. Soc.* **1985**, *107*, 7093−7097.

(33) (a) Bhasikuttan, A. C.; Singh, A. K.; Palit, D. K.; Sapre, A. V.; Mittal, J. P. *J. Phys. Chem. A* **1998**, *102*, 3470−3480. (b) Singh, A. K.; Bhasikuttan, A. C.; Palit, D. K.; Mittal, J. P. *J. Phys. Chem. A* **2000**, *104*, 7002−7009.

(34) (a) Mitsui, M.; Ohshima, Y. *J. Phys. Chem. A* **2000**, *104*, 8638−8648. (b) Mitsui, M.; Ohshima, Y.; Ishiuchi, S.-i.; Sakai, M.; Fujii, M. *J. Phys. Chem. A* **2000**, *104*, 8649−8659. (c) Mitsui, M.; Ohshima, Y.; Kajimoto, O. *J. Phys. Chem. A* **2000**, *104*, 8660−8670.

(35) (a) Morlet-Savary, F.; Ley, C.; Jacques, P.; Wieder, F.; Fouassier, J. P. *J. Photochem. Photobiol. A: Chem.* **1999**, *126*, 7−14. (b) Ley, C.; Morlet-Savary, F.; Jacques, P.; Fouassier, J. P. *Chem. Phys.* **2000**, *255*, 335−346.

(36) Cavaleri, J. J.; Prater, K.; Bowman, R. M. *Chem. Phys. Lett.* **1996**, *259*, 495−502.

(37) van der Burgt, M. J.; Jansen, L. M. G.; Huizer, A. H.; Varma, C. A. G. O. *Chem. Phys.* **1995**, *201*, 525−538.

(38) Hamanoue, K.; Nakayama, T.; Yamaguchi, T.; Ushida, K. *J. Phys. Chem.* **1989**, *93*, 3814−3818.

(39) (a) Scaiano, J. C. *J. Am. Chem. Soc.* **1980**, *102*, 7747−7753. (b) Cosa, G.; Purohit, S.; Scaiano, J. C.; Bosca, F.; Miranda, M. A. *Photochem. Photobiol.* **2002**, *75*, 193−200.

(40) Dalton, J. C.; Montgomery, F. C. *J. Am. Chem. Soc.* **1974**, *96*, 6230−6232.

(41) Rusakowicz, R.; Byers, G. W.; Leermakers, P. A. *J. Am. Chem. Soc.* **1971**, *93*, 3263−3266.
(42) Palit, D. K. *Res. Chem. Intermed.* **2005**, *31*, 205−225.
(43) Tolbert, L. M.; Solntsev, K. M. *Acc. Chem. Res.* **2002**, *35*, 19−27.
(44) Ramseier, M.; Senn, P.; Wirz, J. *J. Phys. Chem. A* **2003**, *107*, 3305−3315.
(45) Li, M-D; Ma, J.; Su, T.; Liu, M. Y.; Yu, L. H.; Phillips, D. L. *J. Phys. Chem. B* **2012**, *116*, 5882−5887.
(46) Du, Y.; Xue, J. D; Li, M. D.; Phillips, D. L. *J. Phys. Chem. A* **2009**, *113*, 3344−3352.